JOURNAL OF AIRCRAFT
Vol. 35, No. 3, May–June 1998

Modal-Based Enhancement of Integrated Design Optimization Schemes

Mordechay Karpel*
Technion—Israel Institute of Technology, Haifa 32000, Israel

The modal approach to integrated structural optimization of aircraft structures offers huge computational savings with acceptable loss of accuracy. The addition of the modal option to existing full-order discrete-coordinate optimization schemes is shown in this paper to provide a very flexible design tool with improved cost effectiveness in typical aerospace design cases. Extensive changes in the modal-based formulation are introduced to expand the scope of its applicability, particularly in the static disciplines. Fictitious masses are used to account for local effects caused by concentrated loads. High-order modal perturbations are introduced for improved accuracy with large move limits. An optional hybrid approach allows the use of modal aeroelastic trim with subsequent discrete-coordinate stress/strain analysis. The new formulation includes the necessary sensitivity analysis for an adequate application in conjunction with the modeling tools of the discrete approach. Tradeoff studies with a realistic generic fighter aircraft model demonstrate the new capabilities.

Nomenclature

$[A]$	= generalized aerodynamic force coefficient matrix
$[FM]$	= matrix of fictitious masses, Eq. (3)
$[K]$	= stiffness matrix
$[LHS]$	= left-side matrix in trim, Eq. (12)
$[M]$	= mass matrix
n_{dv}	= number of design variables
n_h	= number of modal coordinates
n_r	= number of rigid-body modes
$\{\boldsymbol{P}\}$	= vector of external net loads
$[P_1]$, $[P_2]$, $[P_3]$	= aerodynamic load matrices, Eq. (13)
q	= dynamic pressure
$[RHS]$	= right-side matrix in trim, Eq. (12)
$[SU]$	= stress coefficient matrix, Eq. (16)
$\{\boldsymbol{u}\}$	= discrete displacement vector
$\{\boldsymbol{u}\}_0$	= baseline displacements under modified loads, Eq. (19)
v	= design variable
$\{\boldsymbol{\Delta P}\}_i$	= defined in Eq. (30)
$\{\boldsymbol{\Delta u}\}$	= displacements caused by stiffness changes
$\{\boldsymbol{\delta}\}$	= vector to trim variables
$\{\delta \boldsymbol{P}\}_i$	= defined in Eq. (31)
$[\Lambda]$	= eigenvalues of the baseline structure
$[\tilde{\Lambda}]$	= eigenvalues obtained from fictitious-mass modes, Eq. (7)
$\{\boldsymbol{\xi}\}$	= generalized displacement vector
$\{\sigma\}$	= element stresses
$[\phi]$	= normal modes
$[\bar{\phi}]$	= rigid-body modes, Eq. (2)
$[\tilde{\phi}]$	= normal modes recovered from fictitious-mass modes, Eq. (6)
$[\Psi_0]$	= defined in Eq. (20)
$[\psi]$	= eigenvector matrix in generalized coordinates, Eq. (7)

Subscripts

a	= analysis (a-set) coordinates; see Appendix
b	= baseline structure
e	= elastic modal coordinates
f	= free (f-set) coordinates
g	= global (g-set) coordinates
h	= modal coordinates
i, j	= indices of design variables
l	= left (l-set) coordinates after removing r-set ones
MD	= mode-displacement method
r	= rigid-body reference (r-set) coordinates
SOF	= summation of force method
δ	= trim variables

Superscripts

(k)	= approximation order
1	= with fictitious masses

Introduction

SEVERAL structural design optimization schemes that can deal with large-order finite element (FE) models under various types of design constraints were developed in recent years. An example is the Automated Structural Optimization System (ASTROS)[1] that was developed to provide a multidisciplinary analysis and design capability for aerospace structures. The considered disciplines include static response under fixed loads, static aeroelasticity, dynamic response, flutter, and some features of the interaction with control systems. Other finite element analysis and optimization schemes that deal with these disciplines were presented by Haftka,[2] Climent and Johnson,[3] and Bindolino et al.[4]

The dynamic response and stability analyses are treated in these schemes by the modal approach, but the static aeroelastic and stress disciplines are treated by the full-order discrete approach. Each iteration starts with the reconstruction of full-order stiffness and mass matrices, followed by a new normal-mode analysis for the dynamic disciplines and new cost function, constraints, and sensitivity calculations. A constrained-function minimization scheme, such as MICRO-DOT,[5] is then used to progress toward an optimum within prescribed move limits. The task of multidisciplinary optimization for a realistic aircraft design may require computer runs of large CPU time (several hours with current workstations). The resulting turnaround time puts severe limits on the number of

Presented as Paper 96-4126 at the AIAA/USAF/NASA/ISSMO 6th Symposium on Multidisciplinary Analysis and Optimization, Bellevue, WA, Sept. 4–6, 1996; received Dec. 7, 1996; revision received July 7, 1997; accepted for publication Dec. 17, 1997.

*Associate Professor, Faculty of Aerospace Engineering. Member AIAA.

design trials and trade studies that can be performed in an actual design process.

The desire for more efficient procedures for the optimal design of complex structures motivated the development of reduced-size methods. Livne et al.[6] used the equivalent-plate approach of Giles,[7] which grossly reduces the number of structural degrees of freedom but is not as general as the finite element approach, and it requires separate modeling efforts. Karpel and Sheena[8] used the modal approach, where calculations of all the response and stability parameters and their sensitivity to changes in the design variables are based on a set of low-frequency vibration modes of a baseline structure. The modal approach is particularly attractive in multidisciplinary cases where the excitation loads are affected by the structural response, such as in aeroelastic and control augmented systems. The static part of Ref. 8 included aeroelastic effectiveness only, based on the modal scheme of Karpel.[9] It was later extended to deal with static stress constraints by using a modal-perturbation scheme.[10]

The optimization schemes of Refs. 8–10 were based on a modal database that was generated for the baseline structure by common finite element codes such as NASTRAN. The modal optimization scheme was then employed in a separate code that performed a major optimization cycle, including updating the generalized matrices, repeated analyses, sensitivity computations, and design steps, with the database modal information only. The final design variables were then used to modify the FE model for a final analysis or for a new optimization cycle.

The first implementation of the modal approach as an option in a discrete-coordinate optimization code with static aeroelastic and stress constraints is reported in Ref. 11. This implementation was performed with the ASTROS code.[12] It involved some formulation changes for compatibility with the ASTROS methodology and modeling options but the basic modal analysis and sensitivity formulation was similar to that of Ref. 10. A numerical example of a generic fighter aircraft with about a 4000 degree-of-freedom FE model demonstrated the performance of the modal approach, with 40 lowest-frequency normal modes of the free–free aircraft taken into account, in comparison with the regular discrete approach. Optimization runs were performed with wing-skin changes of up to 30%. The most significant effect of the modal approach was in the aeroelastic trim part (which was the most time-consuming part of the regular runs), with speed-up factors of about 80, and error levels of less than 1%. The speed-up factors in the subsequent stress part were about 4, with stress errors up to 10%.

The implementation of the discrete and modal approaches in one code calls for further developments in two aspects: 1) combining parts of the two formulations for more cost-effective and flexible algorithms, and 2) expanding the scope of the modal approach to facilitate seamless integration that supports all of the modeling options. The purpose of this paper is to present new developments in static analysis that support and improve the modal-based enhancement of integrated optimization schemes and their implementation in ASTROS.

Modal Coordinates and Matrices

The ASTROS[12] definition of discrete coordinate sets (which are identical to those of NASTRAN) and the associated FE stiffness and mass matrices are discussed in detail in Ref. 12 and are briefly given in the Appendix. The modal coordinates are based on an eigensolution of the structural analysis (a set) matrices $[K_{aa}]$ and $[M_{aa}]$ of the baseline structure. The resulting set of normal modes satisfy the eigenvalue problem

$$[K_{aa}][\phi_a] = [M_{aa}][\phi_a][\lambda] \tag{1}$$

where $[\lambda]$ is a diagonal matrix of the corresponding eigenvalues, where the first n_r rigid-body values are zero.

The basic assumption of the modal approach in structural optimization is that the displacements (static or dynamic) of the modified structure in response to external excitation can be adequately expressed as a linear combination of the baseline modes

$$\{\boldsymbol{u}_a\} = [\bar{\phi}_{ar}]\{\boldsymbol{\xi}_r\} + [\phi_{ae}]\{\boldsymbol{\xi}_e\} \tag{2}$$

where $\{\boldsymbol{\xi}_r\}$ and $\{\boldsymbol{\xi}_e\}$ are vectors of the generalized displacements, $[\phi_{ae}]$ is the matrix of n_e low-frequency elastic modes taken into account, and $[\bar{\phi}_{ar}]$ is the matrix of n_r rigid-body modes defined by imposing sequential unit displacements at the rigid-body reference displacements $\{\boldsymbol{u}_r\}$ (which is a subset of $\{\boldsymbol{u}_a\}$). The orthogonal rigid-body modes in $[\phi_a]$ of Eq. (1) are replaced by $[\bar{\phi}_{ar}]$ because the latter are not affected by the mass distribution.

The modified modal approach allows the use of relatively large fictitious-mass (FM) elements that cause local deformations, around the points of their application, in the modal coordinates. A general presentation of the use of fictitious-mass elements in structural dynamics is given in Ref. 13. An application to cases of concentrated loads is given in Ref. 14. The modified modal approach first calculates a set of low-frequency normal modes with the nominal mass matrix $[M_{aa}]$ replaced by

$$[M^1_{aa}] = [M_{aa}] + [FM_{aa}] \tag{3}$$

where $[FM_{aa}]$ is a zero matrix except for fictitious mass terms at a small number of selected points, where relatively large concentrated loads are anticipated. The resulting set of n_h low-frequency normal modes $[\phi^1_a]$ and the associated eigenvalues $[\lambda^1]$ yield the associated diagonal generalized mass and stiffness matrices of the FM-modified structure

$$[M^1_{hh}] = [\phi^1_a]^T[M^1_{aa}][\phi^1_a] \tag{4}$$

$$[K^1_{hh}] = [\phi^1_a]^T[K_{aa}][\phi^1_a] = [M^1_{hh}][\lambda^1] \tag{5}$$

The basic assumption of the fictitious-mass approach is that the actual displacement vector $\{\boldsymbol{u}_a\}$ is a linear combination of the fictitious-mass modes $[\phi^1_a]$. To allow a convenient application of fictitious masses in standard finite element codes, we replace $[\phi^1_a]$ by another set of n_h modes $[\tilde{\phi}_a]$, which corresponds to the nominal $[M_{aa}]$, but its vectors are linear combinations of $[\phi^1_a]$, namely,

$$[\tilde{\phi}_a] = [\phi^1_a][\psi] \tag{6}$$

where $[\psi]$ is an $n_h \times n_h$ square nonsingular matrix, which means that this is a transformation that does not lose any information. The substitution of Eq. (6) in Eq. (1), premultiplication by $[\phi^1_a]^T$, and the use of Eqs. (3–5) yield the eigenvalue problem

$$[K^1_{hh}][\psi] = ([M^1_{hh}] - [\phi^1_a]^T[FM_{aa}][\phi^1_a])[\psi][\tilde{\lambda}] \tag{7}$$

which is easily solved for all of the n_h eigenvalues $[\tilde{\lambda}]$ and the associated square eigenvector matrix $[\psi]$. The resulting $[\psi]$ is used to calculate $[\tilde{\phi}_a]$ by Eq. (6).

The low eigenvalues in $[\tilde{\lambda}]$ and the associated modes in $[\tilde{\phi}_a]$ are typically almost identical to those of the nominal FE model. The highest-frequency modes reflect local deformations (around the degrees of freedom loaded by fictitious masses) and are not necessarily actual natural modes. They are requested, however, to account for local deformations in subsequent analyses. From this point on we simply use the n_e elastic modes in $[\tilde{\phi}_a]$ in lieu of $[\phi_{ae}]$ in Eq. (2) and replace the cor-

responding diagonal generalized mass and stiffness matrices of the baseline structure by

$$[M_{ee}]_b = [\psi]^T([M^1_{hh}] - [\phi^1_a]^T[FM_{aa}][\phi^1_a])[\psi] \quad (8)$$

$$[K_{ee}]_b = [M_{ee}]_b[\tilde{\lambda}] \quad (9)$$

Except for the local deformations in some modal coordinates the effect of the fictitious masses has been removed, and we return to the regular modal-based process with the basic assumption of Eq. (2).

The rigid-body mass matrix with respect to $\{u_r\}$ and the mass coupling matrix are

$$\begin{bmatrix} M_{rr} \\ M_{er} \end{bmatrix}_b = [\bar{\phi}_{ar}\ \phi_{ae}]^T[M_{aa}]_b[\bar{\phi}_{ar}] \quad (10)$$

where $[M_{er}]_b = 0$ and $[M_{rr}]$ is a full matrix. When we use the baseline modes as generalized coordinates of a modified structure, $[K_{ee}]$ and $[M_{ee}]$ become full matrices as well, and $[M_{er}]$ becomes nonzero. The generalized matrix updates are based on the sensitivity matrices $\partial[K_{ee}]/\partial v_i$, $\partial[M_{rr}]/\partial v_i$, and $\partial[M_{er}]/\partial v_i$. These sensitivity matrices are calculated by pre- and postmultiplication of the discrete g-set matrices in the Appendix by the baseline modes and are stored in the database before the design process starts.

Aeroelastic Equilibrium Equations

The use of modal coordinates in the construction and solution of the generalized static and static–aeroelastic equilibrium equations is presented in detail in Ref. 11. The most general case is static aeroelastic equilibrium for a free structure

$$\begin{bmatrix} -qA_{rr} & -qA_{re} & M_{rr} \\ -qA_{er} & K_{ee} - qA_{ee} & M_{er} \\ M_{rr} & M^T_{er} & 0 \end{bmatrix} \begin{Bmatrix} \xi_r \\ \xi_e \\ \ddot{\xi}_r \end{Bmatrix} = \begin{bmatrix} qA_{r\delta} \\ qA_{e\delta} \\ 0 \end{bmatrix} \{\delta\} \quad (11)$$

where $\{\delta\}$ includes trim variables such as angle of attack and control-surface deflection. The elimination of $\{\xi_r\}$ and $\{\xi_e\}$ yields the aeroelastic trim equation

$$[LHS]\{\ddot{\xi}_r\} = [RHS]\{\delta\} \quad (12)$$

All of the parameters in $\{\ddot{\xi}_r\}$ and $\{\delta\}$ are defined by the user, except for n_r variables that are solved for by Eq. (12). Equation (11) is then solved for $\{\xi_r\}$ and $\{\xi_e\}$. These aeroelastic solutions can be performed for either prescribed aircraft maneuvers or for aeroelastic effectiveness constraints. Analytical expressions for the derivatives of equilibrium variables and the effectiveness parameters, with respect to the design variables v_i, are given in Ref. 11.

The data needed for trim and effectiveness analysis along an optimization path include only the generalized structural and aerodynamic matrices of Eq. (11) and the derivatives of the generalized structural matrices with respect to v_i. This is a relatively small amount of data that can be easily exported for use by a separate code. Reference 8 used these data for structural optimization with aeroelastic effectiveness constraints only. The optimization scheme of Ref. 9 used these data for optimization with aeroelastic effectiveness, flutter, and control-margin constraints. Major design optimization studies were carried out in these applications by extremely efficient runs (typically less than 30 s per design iteration on a MicroVax workstation). The end results were then used to update the full FE models for a final verification.

Loads and Stress by the Hybrid Approach

The application of stress constraints requires the recovery of the full g-set displacement vector $\{u_g\}$ after the trim equations are solved and then the application of stress-displacement relationships. Reference 10 showed that displacements obtained by the basic assumption in Eq. (2) may be adequate for stress evaluation only with the baseline structure. Stress analysis of the modified structure, while using the baseline modes as generalized coordinates, required modal perturbation matrices that contain local deformations caused by unit changes in the design variables. On the other hand, Refs. 10 and 14 showed that the modal aeroelastic solution can still be adequate for calculating the external net loads on the trimmed aircraft throughout the optimization process by

$$\{P_a\} = [P_1]\{\delta\} + [P_2]\{\xi_r\} + [P_3]\{\xi_e\} - [M_{aa}][\bar{\phi}_{ar}]\{\ddot{\xi}_r\} \quad (13)$$

where the inertia relief term does not actually require the update of $[M_{aa}]$. Instead, it can be based on the components of $[M_{gg}]$ using the recovery/reduction process described in the Appendix, starting with $\{\ddot{u}_a\} = [\bar{\phi}_{ar}]\{\ddot{\xi}_r\}$. The modal-approach stress analyses in the following sections use this process for all the mass- and stiffness-dependent load vectors.

The derivatives of the variable vectors in the right side of Eq. (13) can be used to calculate the load sensitivity $\partial\{P_a\}/\partial v_i$, taking into account that the only coefficient matrix in Eq. (13) that varied with the design variables is $[M_{aa}]$.

The most accurate way to perform stress analysis at this point is by returning to the full FE model with the loads of Eq. (13), as done for example by Huang et al.[15] Because the stiffness matrix $[K_{aa}]$ is singular the model is supported by eliminating the terms associated with $\{u_r\}$, and the displacements are calculated by

$$\{u_l\} = [K_{ll}]^{-1}\{P_l\} + [\bar{\phi}_{lr}]\{u_r\} \quad (14)$$

where $\{u_r\}$ is calculated by the respective row partition of Eq. (2)

$$\{u_r\} = \{\xi_r\} + [\phi_{re}]\{\xi_e\} \quad (15)$$

The displacements of Eqs. (14) and (15) are merged for $\{u_a\}$ and then expanded to obtain the global (g-set) displacement vector $\{u_g\}$ by the regular discrete-coordinate recovery process.[12] Element stresses are calculated by

$$\{\sigma\} = [SU]\{u_g\} \quad (16)$$

where $[SU]$ is a fixed matrix.

The differentiation of Eqs. (14) and (15) yields the displacement sensitivity

$$\frac{\partial\{u_l\}}{\partial v_i} = [K_{ll}]^{-1}\left(\frac{\partial\{P_l\}}{\partial v_i} - \frac{\partial[K_{ll}]}{\partial v_i}\{u_l\}\right) + [\bar{\phi}_{lr}]\frac{\partial\{u_r\}}{\partial v_i} \quad (17)$$

where

$$\frac{\partial\{u_r\}}{\partial v_i} = \frac{\partial\{\xi_r\}}{\partial v_i} + [\phi_{re}]\frac{\partial\{\xi_e\}}{\partial v_i} \quad (18)$$

Stress sensitivities are based on the derivatives of $\{u_g\}$ that are recovered from $\partial\{u_l\}/\partial v_i$.

The hybrid approach is easy to implement when the modal and discrete schemes are integrated in one code. It might still be very inefficient, however, with large models.

Modal Stress Approximations

The numerical advantages of performing modal-based design optimization without returning to the full FE model motivated the development of a modal-based stress-analysis method.[10] The basic idea was that even though displacements calculated by Eq. (2) cannot be used for stresses of the mod-

ified structure, they can still be used for stresses of the baseline structure and for a zero-order guess of the internal loads applied by the added material. The displacement vector for stress analysis is composed by

$$\{u_l\} = \{u_l\}_0 + \{\Delta u\} + [\bar{\phi}_{lr}]\{u_r\} \tag{19}$$

where $\{u_l\}_0$ is the elastic displacement of the baseline structure under the modified net loads, relative to $\{u_r\}$, $\{\Delta u\}$ reflects the change of the displacements caused by stiffness changes, and the last term is the same rigid-body shift (which does not affect stresses) as in Eq. (14).

New expressions for the first two right-side terms of Eq. (19) and their derivatives with respect to the design variables are given next. The new options allow greater flexibility and higher accuracy when the modal approach is integrated with a discrete scheme. Following the calculation of $\{u_l\}$ we can recover $\{u_g\}$ and calculate stresses by Eq. (16).

Baseline Structure Under Modified Loads

The first term of Eq. (19) is based in Ref. 10 on the mode-displacement (MD) approach, which yields

$$\{u_l\}_{0_{MD}} = ([\phi_{le}] - [\bar{\phi}_{lr}][\phi_{re}])[\Psi_0]\{\xi_e\} \tag{20}$$

where

$$[\Psi_0] = [I] + [K_{ee}]_b^{-1}\left[\sum_{i=1}^{n_{dv}} (v_i - v_{b_i})\frac{\partial[K_{ee}]}{\partial v_i}\right]$$

The differentiation of Eq. (20) gives

$$\frac{\partial\{u_l\}_{0_{MD}}}{\partial v_i} = ([\phi_{le}] - [\bar{\phi}_{lr}][\phi_{re}])\left([\Psi_0]\frac{\partial\{\xi_e\}}{\partial v_i} + [K_{ee}]_b^{-1}\frac{\partial[K_{ee}]}{\partial v_i}\right) \tag{21}$$

The main advantage of the MD displacements and their derivatives is that their computation is very efficient and does not require the explicit computation of the external loads of Eq. (13). A somewhat less efficient but more accurate way to calculate $\{u_l\}_0$ is by extracting these loads and then applying them to the baseline stiffness matrix $[K_{ll}]_b$. This summation-of-force (SOF) way is particularly feasible when the modal and discrete codes are integrated, mainly because $[K_{ll}]_b$ is available in core and has already been decomposed when the modes were calculated. The SOF expression for $\{u_l\}_0$ is simply

$$\{u_l\}_{0_{SOF}} = [K_{ll}]_b^{-1}\{P_l\} \tag{22}$$

and its sensitivity is

$$\frac{\partial\{u_l\}_{0_{SOF}}}{\partial v_i} = [K_{ll}]_b^{-1}\frac{\partial\{P_l\}}{\partial v_i} \tag{23}$$

First-Order Displacement Increment

The second term in Eq. (19), $\{\Delta u\}$, is an approximation of the displacement changes as a result of forces applied by the added material on the baseline structure. The basic modal assumption of Eq. (2) provides a good initial guess for the total elastic deformations

$$\{u_l^{(0)}\} = [\phi_{le}]\{\xi_e\} \tag{24}$$

which is recovered to the g set and used to calculate the first-order approximation of $\{\Delta u\}$ by

$$\{\Delta u^{(1)}\} = [K_{ll}]_b^{-1}\left[\sum_{i=1}^{n_{dv}} (v_i - v_{b_i})[\phi_{Fl}]_i\right]\{\xi_e\} \tag{25}$$

where $[\phi_{Fl}]_i$ is the l-set reduction of

$$[\phi_{Fg}]_i = -\frac{\partial[K_{gg}]}{\partial v_i}[\phi_{ge}] \tag{26}$$

The differentiation of Eq. (25), considering Eqs. (24) and (26), gives

$$\frac{\partial\{\Delta u^{(1)}\}}{\partial v_i} = [K_{ll}]_b^{-1}\left([\phi_{Fl}]_i\{\xi_e\} + \left[\sum_{j=1}^{n_{dv}} (v_j - v_{b_j})[\phi_{Fl}]_j\right]\frac{\partial\{\xi_e\}}{\partial v_i}\right) \tag{27}$$

Equation (19), with $\{u_l\}_0$ of either Eq. (20) or (22), $\{\Delta u^{(1)}\}$ of Eq. (26), and $\{u_r\}$ of Eq. (15) gives the first-order approximation of $\{u_l\}$. Its sensitivities to the design variables are calculated by the respective derivatives in Eqs. (21) or (23), (27), and (18). The first use of modal stresses in structural optimization[10] was in a separate code that received modal data from NASTRAN. The MD approach was taken for $\{u_l\}_0$, and $\{\Delta u^{(1)}\}$ and its derivatives were calculated with the products $[K_{ll}]_b^{-1}[\phi_{Fl}]_i$ calculated in advance by NASTRAN and saved in the database as modal perturbations (one for each design variable). In this way, there was no need to export the large discrete-coordinate stiffness matrices to the optimization code. A later application of the modal approach in ASTROS[11] still followed a similar formulation.

High-Order Approximations

Starting with $k = 1$, a kth-order approximation $\{u_l^{(k)}\}$ can be used for calculating a higher-order version of Eq. (19)

$$\{u_l^{(k+1)}\} = \{u_l\}_0 + \{\Delta u^{(k+1)}\} + [\bar{\phi}_{lr}]\{u_r\} \tag{28}$$

where $\{\Delta u^{(k+1)}\}$ is calculated by

$$\{\Delta u^{(k+1)}\} = [K_{ll}]_b^{-1}\left(\sum_{i=1}^{n_{dv}} (v_i - v_{b_i})\{\Delta P_l^{(k)}\}_i\right) \tag{29}$$

where $\{\Delta P_l^{(k)}\}_i$ is the l-set reduction of

$$\{\Delta P_g^{(k)}\}_i = -\frac{\partial[K_{gg}]}{\partial v_i}\{u_g^{(k)}\} \tag{30}$$

The differentiation of Eq. (29) yields the high-order sensitivities

$$\frac{\partial\{\Delta u^{(k+1)}\}}{\partial v_i} = [K_{ll}]_b^{-1}(\{\Delta P_l^{(k)}\}_i + \{\delta P_l^{(k)}\}_i) \tag{31}$$

where $\{\delta P_l^{(k)}\}_i$ is the l-set reduction of

$$\{\delta P_g^{(k)}\}_i = -\left(\sum_{j=1}^{n_{dv}} (v_j - v_{b_j})\frac{\partial[K_{gg}]}{\partial v_j}\right)\frac{\partial\{u_g^{(k)}\}}{\partial v_i}$$

Numerical Examples

The numerical examples are based on a generic advanced fighter aluminum (AFA) ASTROS model whose aerodynamic model is shown in Fig. 1. The structural model consists of 1276 grid points and 4449 elements and has 3761 free degrees of freedom with symmetric boundary conditions. A top view of the wing structural model is shown in Fig. 2.

The first case is static response of the free aircraft to a concentrated vertical force of 10,000 lb applied to the wing at point (X = 352.5, Y = 117.0) (Fig. 2). The modal solutions were obtained with two rigid-body modes (heave and pitch) and 41 elastic symmetric modes. Equation (11) is applied in this case with no aerodynamics and with the right side replaced by the generalized forces caused by the external force. The

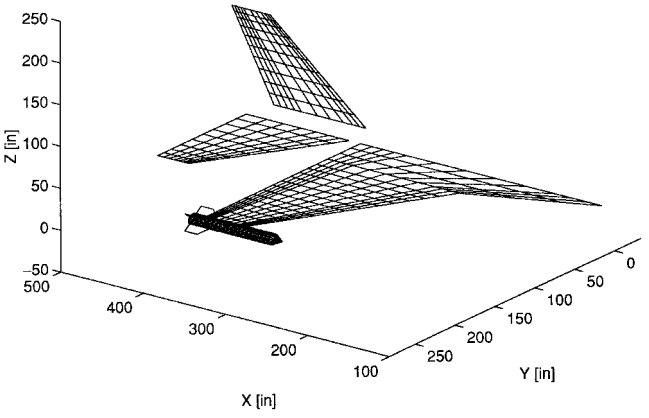

Fig. 1 AFA unified subsonic and supersonic aerodynamic model.

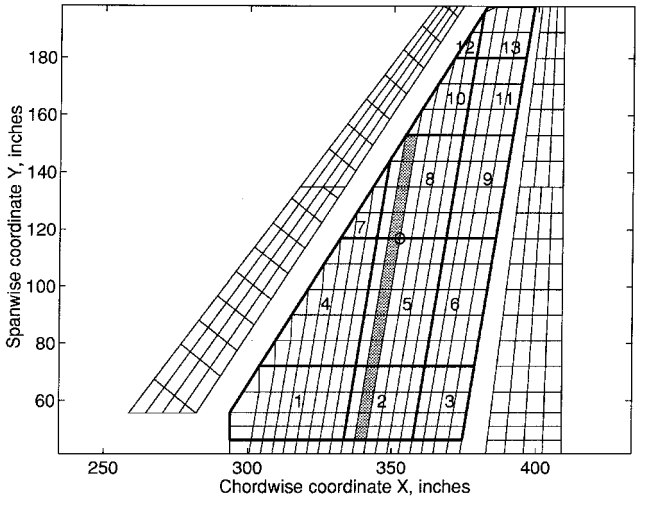

Fig. 2 AFA wing structural model.

structural response includes the effects of the distributed inertia-relief forces. The resulting von Mises stresses along an upper-skin row of elements (the gray area in Fig. 2) and shear stresses along the spar that passes through the force point are shown in Fig. 3. Three solutions are compared: 1) a discrete-coordinate solution, 2) a regular modal solution with no fictitious masses, and 3) a modal solution with one fictitious mass of 1000 lb added to the force point. It is obvious that the modal results without the fictitious mass are unacceptable, particularly near the force point. The fictitious-mass results, on the other hand, are practically identical to those of the discrete solution.

For structural optimization the wing box is divided into 13 zones, as shown in Fig. 2. The thickness values in each zone are multiplied in the optimization process by one factor for the upper skin and one for the lower skin elements, for a total of 26 global design variables. The inner structure of the wing as well as the structure of the rest of the aircraft are not subjected to changes. The aeroelastic database was constructed with the same set of modes as described earlier for the case of no fictitious masses (as regular maneuver loads are well distributed). The optimization is performed for minimum weight of the wing-box skin, with stress constraints generated by a single case of a symmetric 9-*g* pull-up maneuver at Mach 0.95. The von Mises stresses of the skin elements are constrained to less than the limit of 36,700 psi.

Optimization studies were performed for two different initial skin thickness distributions. Reference runs were first obtained with the standard discrete-coordinate ASTROS code, version 11.0. The skin thickness distributions and the wing-box skin

Table 1 Skin thickness in initial and final designs

	Skin thickness, in.		
	Initial 1	Initial 2	Optimal
Zone			
1*U*	0.80	0.95	0.667
1*L*	0.80	1.00	0.660
2*U*	0.80	0.80	0.709
2*L*	0.80	0.80	0.584
3*U*	0.70	0.70	0.523
3*L*	0.50	0.60	0.408
4*U*	0.45	0.45	0.395
4*L*	0.50	0.65	0.409
5*U*	0.40	0.45	0.343
5*L*	0.30	0.45	0.239
6*U*	0.03	0.10	0.021
6*L*	0.13	0.15	0.095
7*U*	0.45	0.45	0.409
7*L*	0.60	0.60	0.479
8*U*	0.25	0.25	0.210
8*L*	0.20	0.20	0.163
9*U*	0.02	0.08	0.018
9*L*	0.05	0.07	0.029
10*U*	0.20	0.20	0.170
10*L*	0.20	0.20	0.175
11*U*	0.02	0.06	0.017
11*L*	0.02	0.06	0.015
12*U*	0.10	0.25	0.081
12*L*	0.10	0.22	0.073
13*U*	0.10	0.15	0.084
13*L*	0.15	0.17	0.111
Weight, lb	582.8	678.5	481.3

Note: *U*, upper; *L*, lower.

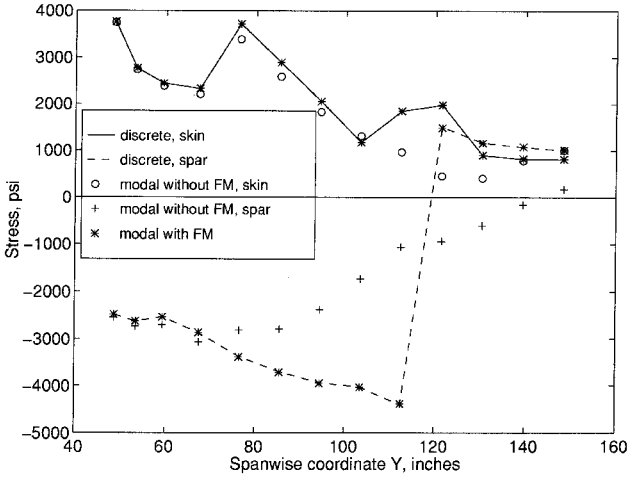

Fig. 3 Stresses because of concentrated excitation.

weight of the two initial wings are compared in Table 1 to those of the optimized structure.

The total wing-box skin weight reduction was 18% in the first case and 30% in the second one. The discrete optimization runs were completed by ASTROS in two design iterations in the first case and three in the second one. In more typical design studies, when there are more disciplines and design cases, the number of iterations is usually much larger. With our simple optimization cases, however, we gain more insight. The variation of the total wing-box skin weight along the optimization path with the first initial design for discrete and modal optimization cases is given in Fig. 4. Three modal-based approach options are shown: 1) The hybrid approach that resorts to discrete formulation once aeroelastic loads are defined, 2) the MD approach that starts with Eq. (20), and 3) the SOF approach that starts with Eq. (22). The weight variations of the MD and SOF approaches are given for first- and second-

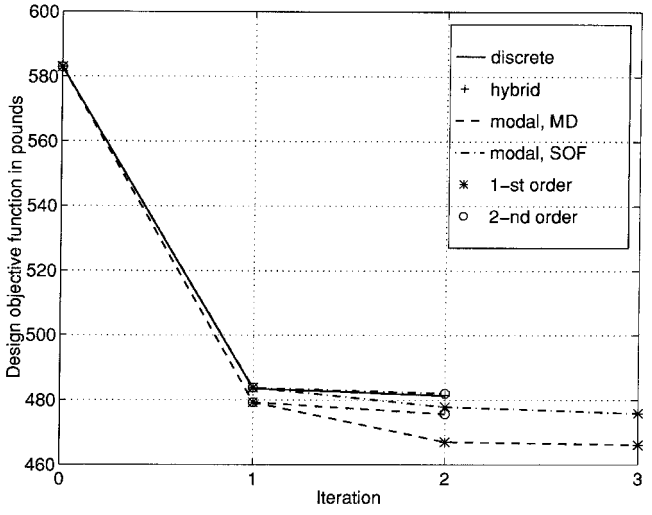

Fig. 4 Weight of the designed skin along the optimization path, first initial design.

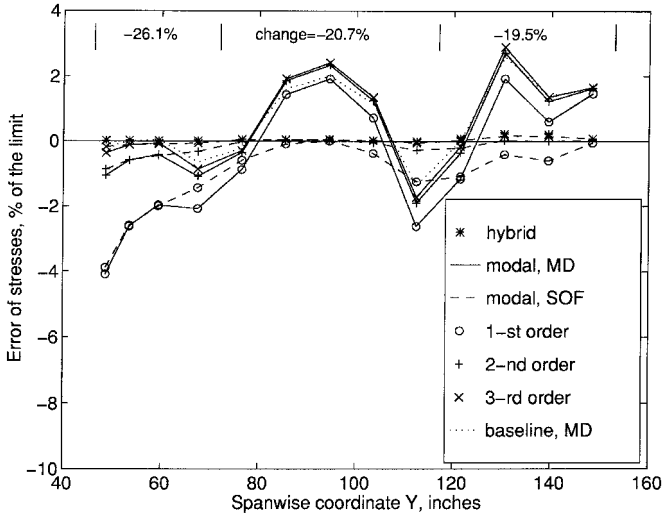

Fig. 5 Percentage stress errors after first design step, first initial design.

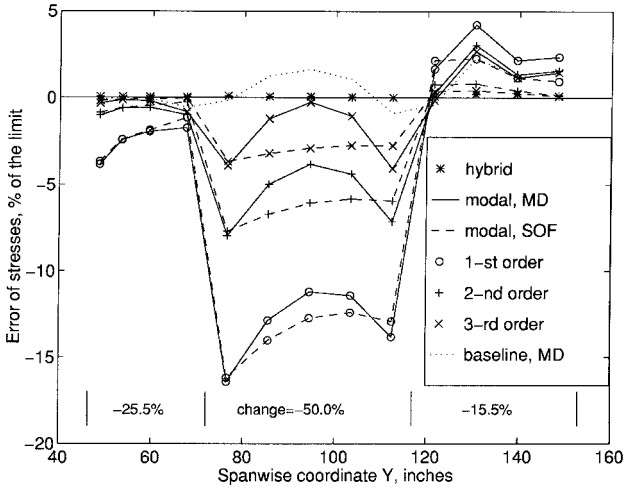

Fig. 6 Percentage stress errors after first design step, second initial design.

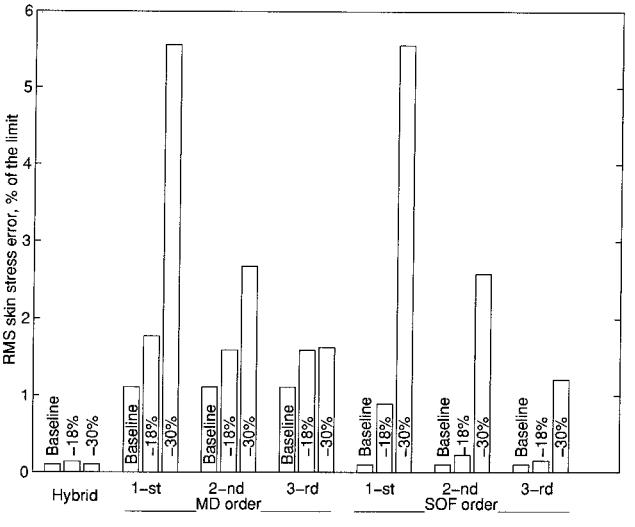

Fig. 7 Root-mean-square percentage stress errors with different update schemes.

order displacement approximations. The hybrid optimization path in Fig. 4 is practically identical to the discrete path. The final weight error of the MD modal approach is −3.1%, compared to the discrete case, for the first-order case, and −1.2% for the second-order case. The errors of the SOF cases are significantly smaller, −1.1 and 0.1%. The optimization paths for the second initial design were similar to those of the first one, but the final weight errors were about 2.5 times larger.

To examine the accuracy of the different modal approaches when the structure changes, the element stresses after the first design change of the discrete optimization process were compared to those calculated by the different modal approaches for these design variables. All of the modal calculations here were based on the data of the first initial structure in Table 1. The modal-based von Mises stress errors along the lower skin elements marked in Fig. 2, in terms of percentage fraction of the limit stress, are shown in Fig. 5. The errors of the MD approach in the baseline design is also shown (the dotted line). As expected, the largest errors are for the MD first-order case that generally tends to underestimate the stresses and, hence, leads to a nonconservative design (see Fig. 4). When the approximation order increases the MD approach converges rapidly to the baseline MD errors. The SOF errors are generally smaller and converge to the errors of the hybrid approach, which are practically zero. The changes indicated at the top of Fig. 5 are those of the design variables associated with the lower skin of zones 2, 5, and 8, relative to the first initial design in Table 1.

The stress cases of Fig. 5 were also evaluated for the second initial design of Table 1 and are shown in Fig. 6. This time the design change in the middle section (−50% at zone 5) is much larger than in the other zones. The general tendency of the stress errors is similar to that of Fig. 5. However, it should be noticed that the stress errors of the first-order modal solutions are unacceptably large, and that the SOF errors are not smaller at this zone than the MD ones, even for third-order approximation. Both methods do not handle such large local design changes very well.

Percentage rms stress errors over the entire wing-box skin are shown in Fig. 7 for the various modal formulations. Errors are given in each case for the first baseline design and for the first set of the discrete-process design changes, as calculated by the modal methods with the data of the first and second initial designs (weight changes of −18 and −30%, respectively). It is clear that the errors of the hybrid approach are negligible. The baseline cases are not affected by the approximation order, with the SOF baseline stresses being identical to the hybrid ones (because SOF formulation is identical to the hybrid one for a baseline structure). Both MD and SOF methods converge to the respective baseline errors quite rapidly with the increased approximation order. The choice of an

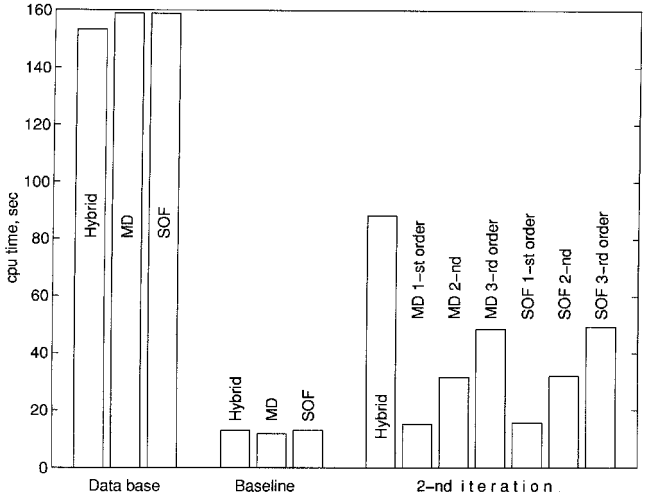

Fig. 8 Comparison of CPU times for various modal optimization schemes.

adequate formulation depends on the application. If, for example, we are satisfied with an rms error level of 1.5% (which is reasonable in extensive preliminary-design studies), we can use the first-order MD approach for design changes of up to 25%, and higher orders for larger changes. SOF approximations will give higher accuracy, but not much higher when the design changes are relatively large (about 50%).

The choice of the adequate method depends, of course, also on its relative numerical efficiency. The computations in this work were performed on an SGI Indigo2 workstation with an R4400 processor. A detailed breakdown of the CPU time for an MD first-order case performed with the same model of this paper, in comparison with the discrete-coordinate optimization, is given in Ref. 11. A comparison between the CPU time consumed by the different model update and sensitivity schemes of this paper in the database and design phases is shown in Fig. 8. The time for the modal database construction is mainly for calculating the normal modes. The database time given in Fig. 8 is with the normal-mode CPU time when using the Lanczos method, as utilized in NASTRAN. The CPU time for all methods is almost identical when applied to the baseline structure. Subsequent iterations, however, are much more efficient with the MD formulation. The regular discrete approach (not shown) does not spend any time on constructing a modal database, but spends 393 s in each iteration. When applied with control effectiveness constraints only, the discrete approach took 387 s/iteration, while the modal approach took only 5 s /iteration after the database construction.[11]

Conclusions

Several modal-based reanalysis and sensitivity formulations were implemented in the ASTROS discrete-coordinate module for optimization with static aeroelastic and stress constraints under static maneuver loads. The implementation facilitates a significant improvement of the code's cost effectiveness. The improvement is most dramatic in the static aeroelastic equilibrium and effectiveness part, where the modal results are practically perfect and the CPU gains per iteration are of almost two orders of magnitude. A typical CPU time for constructing a modal database for a given set of boundary conditions and performing the first design step with stress constraints was about 45% of a single discrete-coordinate step. The CPU time for subsequent iterations was between 4%, for the first-order mode-displacement approach, and 22% for the hybrid approach that returns to the discrete procedure after the aeroelastic trim equations are solved. Regular aircraft maneuver cases can be applied with about 40 elastic modes of the entire aircraft. Extreme concentrated loads can be adequately treated by the application of fictitious masses.

Appendix: Discrete Coordinates and Matrices

Common finite element codes such as NASTRAN start the construction of the structural matrices at the individual element level. The contribution of each element is transformed to the global (g-set) coordinate system, which contains six coordinates for each grid point, and added to the g-set stiffness and mass matrices, $[K_{gg}]$ and $[M_{gg}]$, respectively. At this preface stage, the matrices are not affected by modeling constraints, boundary conditions, or solution methods.

To avoid repetitive construction of the g-set matrices from scratch, the ASTROS optimization code separates the contributions of the structural parts that are affected by the n_{dv} global design variables from those that are not affected. A global design variable is a changeable factor that multiplies the structural matrices of a user-defined group of finite elements. In each design cycle, the matrices are assembled by adding the contributions of the changeable elements to the contribution of the fixed elements. The stiffness matrix is assembled by

$$[K_{gg}] = [K_{gg}]_0 + \sum_{i=1}^{n_{dv}} v_i \frac{\partial [K_{gg}]}{\partial v_i}$$

and the mass matrix by

$$[M_{gg}] = [M_{gg}]_0 + \sum_{i=1}^{n_{dv}} v_i \frac{\partial [M_{gg}]}{\partial v_i}$$

where v_i is the current value of the ith design variable. These equations assume linear contributions of the design variables. The contributions of most finite elements in typical aerospace models are indeed linear with respect to a representative gauge. ASTROS also supports bar and plate elements, whose contributions to the g-set stiffness matrix are proportional to a power of v_i. These elements are omitted here for clarity and simplicity.

The g-set matrices are reduced to the free (f-set) coordinates by application of single- and multipoint constraints (SPC and MPC). This reduction to $[K_{ff}]$ and $[M_{ff}]$ is repeated in each discrete-coordinate design iteration. ASTROS defines these constraints as boundary conditions and allows simultaneous optimization runs with different sets of boundary conditions.

NASTRAN and ASTROS allow a further reduction of the structural matrices by Guyan's static condensation.[11] The resulting analysis (a-set) coordinates and the associated $[K_{aa}]$ and $[M_{aa}]$ are used for normal-modes and static equilibrium analyses, after which the response at the omitted (o-set) coordinates can be recovered. The transformation matrices are functions of the stiffness properties and should be recalculated in each design iteration. Static condensation is not very effective when modern numerical solution methods, such as the Lanczos method for eigensolutions, are used. The condensation can still be effective, however, when large structural components are kept unchanged in a design study. If all of the interface coordinates with other parts remain in the a-set, the submatrices associated with the unchanged components are constant throughout the design process.

A further reduction is required when the structure has n_r rigid-body degrees of freedom. User-selected n_r a-set coordinates are used to represent the rigid-body (r-set) motion, whereas the leftover (l-set) coordinates define the relative elastic deformations. While $[K_{aa}]$ is a singular matrix (when $n_r > 0$), $[K_{ll}]$ is not and, hence, can be inverted.

The transformation matrices between the coordinate sets are saved in the database at the initial analysis phase for subsequent recovery of the displacements from the lowest l-set level to the highest g-set level and for reduction of g-set loading vectors to lower sets. The modal approach, which does not update the discrete-coordinate stiffness and mass matrices in each design step, uses a recovery/reduction process to calculate stiffness or mass-dependent loading vectors. To calculate

the inertia loads $\{\boldsymbol{P}_a\} = [M_{aa}]\{\ddot{\boldsymbol{u}}_a\}$, for example, $\{\ddot{\boldsymbol{u}}_a\}$ is first expanded to the g-set $\{\ddot{\boldsymbol{u}}_g\}$, multiplied by the components of $[M_{gg}]$ given earlier, summed according to the current values of the design variables, and then reduced to the a-set level.

Acknowledgments

This work was partially supported by a contract with Lockheed Martin Tactical Aircraft Systems. The numerical applications of this paper were performed with the help of Boris Moulin of the Technion—Israel Institute of Technology.

References

[1]Neill, D. J., Johnson, E. H., and Confield, R., "ASTROS—A Multidisciplinary Automated Structural Design Tool," *Journal of Aircraft*, Vol. 27, No. 12, 1990, pp. 1021–1027.

[2]Haftka, R. T., "Structural Optimization with Aeroelastic Constraints," *International Journal of Vehicle Design*, Vol. 7, No. 3–4, 1986, pp. 381–392.

[3]Climent, H., and Johnson, E. H., "Aeroelastic Optimization Using MSC/NASTRAN," *Proceedings of the International Forum on Aeroelasticity and Structural Dynamics* (Strasbourg, France), Association Aèronautique et Astronautique de France, Paris, 1993, pp. 1097–1116.

[4]Bindolino, G., Lanz, M., Mantegazza, P., and Ricci, S., "Integrated Structural Optimization in the Preliminary Aircraft Design," *Proceedings of the 17th Congress of the International Council of the Aeronautical Sciences* (Stockholm, Sweden), International Council of the Aeronautical Sciences, Amsterdam, The Netherlands, 1990, pp. 1366–1378.

[5]Vanderplaats, G. N., "An Efficient Feasible Directions Algorithm for Design Synthesis," *AIAA Journal*, Vol. 22, No. 11, 1984, pp. 1633–1640.

[6]Livne, E., Schmit, L. A., and Friedmann, P. P., "Integrated Structure/Control/Aerodynamic Synthesis of Actively Controlled Composite Wings," *Journal of Aircraft*, Vol. 30, No. 3, 1993, pp. 387–394.

[7]Giles, G. L., "Equivalent Plate Analysis of Aircraft Wing Box Structures with General Planform Geometry," *Journal of Aircraft*, Vol. 23, No. 11, 1986, pp. 859–864.

[8]Karpel, M., and Sheena, Z., "Structural Optimization for Aeroelastic Control Effectiveness," *Journal of Aircraft*, Vol. 26, No. 8, 1989, pp. 493–495.

[9]Karpel, M., "Multidisciplinary Optimization of Aeroservoelastic Systems Using Reduced-Size Models," *Journal of Aircraft*, Vol. 29, No. 5, 1992, pp. 939–946.

[10]Karpel, M., and Brainin, L., "Stress Considerations in Reduced-Size Aeroelastic Optimization," *AIAA Journal*, Vol. 33, No. 4, 1995, pp. 716–722.

[11]Karpel, M., Moulin, B., and Love, M. H., "Modal-Based Structural Optimization with Static Aeroelastic and Stress Constraints," *Journal of Aircraft*, Vol. 34, No. 3, 1997, pp. 433–440.

[12]Neill, D. J., Herendeen, D. L., and Venkayya, V. B., "ASTROS Enhancements, Volume III—Theoretical Manual," U.S. Air Force Wright Aeronautical Labs., TR-95-3006, May 1995.

[13]Karpel, M., and Raveh, D., "Fictitious Mass Element in Structural Dynamics," *AIAA Journal*, Vol. 34, No. 3, 1996, pp. 607–613.

[14]Karpel, M., and Presente, E., "Structural Dynamic Loads in Response to Impulsive Excitation," *Journal of Aircraft*, Vol. 32, No. 4, 1995, pp. 853–861.

[15]Huang, X., Haftka, R. T., Grossman, B., and Mason, W. H., "Comparison of Statistical Weight Equations with Structural Optimization of a High Speel Civil Transport," *Proceedings of the AIAA/USAF/NASA/ISSMO 5th Symposium on Multidisciplinary Analysis and Optimization* (Panama City, FL), AIAA, Washington, DC, 1994, pp. 1135–1144.